RESEARCH ON GEOMETRIC INVERSE PROBLEM BASED ON THE FIREFLY CONJUGATE GRADIENT METHOD

Shoubin WANG[1], Yunlong LI[1], Guili PENG[1*], Wenbin XU[1], Xuejun ZHOU[1], Yongqiang Ju[2]

[1]College of Control and Mechanical, Tianjin ChengJian University, Tianjin, 300384, China

[2]China Power Construction Municipal Construction Group, Tianjin, 300457, China

[*] Corresponding author; E-mail: penguili@126.com

In this paper the two-dimensional steady-state heat transfer geometric inverse problem is solved using the Finite Element Method (FEM), Conjugate Gradient Method (CGM), and Firefly Algorithm (FA). Based on the finite element method for solving the forward heat transfer model, and based on continuous iterative optimisation of the conjugate gradient method, the accuracy of the error function of the measured and estimated values is kept within a certain range, so that the geometry of the object under test can be calculated in an inverse way. In the study of the forward problem, the temperature field distribution is solved using circular pipes as the research objects, and the feasibility of applying the finite element method to heat transfer problems is verified. The inverse problem takes the circular tube as the object and considers two different corrosion defects on the inner wall of the circular tube. Simultaneously, the firefly algorithm is introduced based on the conjugate gradient method to stochastically optimize the temperature data and suppress the fluctuation of the inversion result. Numerical experiment results indicate that the method in this paper can perform more accurate geometric shape recognition when there is a certain temperature measurement error or the temperature measurement information is relatively complete.

Key words*: Inverse heat transfer problem; Geometric shape recognition; Conjugate gradient method; Firefly algorithm; Finite element method*

1. Introduction

The geometric inverse problem of heat transfer has broad application prospects. It has applications in the fields such as metallurgical engineering, biological lesion detection, non-destructive testing, and equipment geometry optimization, and has received extensive attention from scholars worldwide[1-5]. At present, in the research of heat transfer problems[6-8], forward problems are usually solved by finite difference, boundary element method, finite element method, and finite volume method; the inversion methods of geometric shapes are mainly based on the Levenberg-Marquardt algorithm, conjugate gradient method, steepest descent method, and decentralized fuzzy inference method (DFIM). Jiang et al. conducted the shape recognition of the inner wall of a two-dimensional cylinder based on boundary element and decentralized fuzzy inference methods[9]. Luo et al. studied the fuzzy inversion of the shape of the inner wall of an industrial kiln[10]. Wang

conducted an inversion study on the geometry of the third type of boundary conditions[11]. Based on the finite element method, Li proposed a new non-iterative inversion algorithm to identify the boundary conditions and geometric shapes in the multi-dimensional steady-state heat conduction problem[12]. Wang et al. used the social particle swarm and conjugate gradient algorithm to identify the two-dimensional steady-state boundary shape[13]. Mei et al. used the finite element method to investigate defect detection[14]. Besides, depending on finite element thermal structure analysis, Sun et al. presented an iterative algorithm to solve the inverse calculation of the cold state of the blade geometry[15]. Fazeli et al. identified the shape and location of the two-dimensional defect in the heat conduction inverse problem using the finite element method and gradient optimization algorithm, and further developed the algorithm and applied it to the two-dimensional multi-connection geometric shape recognition problem[16-17]. Li et al. used the boundary element method and fuzzy inference method to explore the inverse problem of the inner geometry of the two-dimensional heat conduction system[18]. Cheng et al. discussed the application of the heat transfer inversion method in shape recognition, and considered several examples of shape recognition of solid internal voids based on solid surface temperature data[19]. Mosavati et all. solved using a simplified back-ward Monte Carlo method (MCM) for the inverse radiation boundary problem and combined natural convection-radiation considering specular reflectivity and participating media is solved[20-22]. Chen et al. employed the conjugate gradient method to invert the shape of the fouling layer in the two-dimensional forced convection pipeline and discussed the influence of the initial value and error on the inversion result[23]. Fan et al. established a transient heat transfer model for a pipe with internal wall defects with internal heat-passing fluid and researched the influence of temperature measurement errors on the identification of the internal wall boundary through simulation experiments[24]. Partridge et al. reverse-coupled the double reciprocity method (DRM) and genetic algorithm (GA) to obtain the size and location of skin tumors from skin surface temperature measurement[25].

The geometry of the pipe is identified as a typical class of heat transfer inverse problems, the solution of which consists of two main components: the creation and solution of the heat transfer temperature field, and the coupling of the inverse algorithm to the positive problem to solve for the unknown parameters. For forward heat transfer, the finite element method used in this paper solves for the method, which is more adaptable to irregular boundary discretization. The solution of inverse problems has long been a focus of scholarly research. In the introductory section of Chapter 1, the methods mentioned in this paper are broadly classified into two categories: statistical class algorithms and deterministic algorithms to solve heat transfer inverse problems. For example, the classical conjugate gradient algorithm is a deterministic algorithm. This type of algorithmic operation mainly uses the gradient information of the objective function, which can solve the inverse problem well, but relies on the influence of the selection and error of the initial value. The biggest advantage of the statistical class of algorithms is that they do not rely on initial value guesses and theoretically do not fall into local extreme value problems in the inverse process, but the algorithms themselves are large in size and take a long time to operate. The hybrid algorithm proposed in this paper, using the firefly algorithm to optimise the conjugate gradient method, is a good solution to the problems that exist in these two classes of algorithms, and has a much better performance and stability for solving heat transfer inverse problems.

Aiming at the geometric shape recognition problem in the heat conduction system, this paper uses the finite element method to solve the two-dimensional steady-state normal problem, address the

inverse problem with the conjugate gradient algorithm, and introduce the firefly algorithm to optimize the temperature information based on the conjugate gradient algorithm. Consequently, the fluctuations in the inversion process are suppressed to a certain extent, and the stability of the inversion is enhanced.

2. Two-dimensional heat transfer forward problem

2.1. Finite element meshing

This paper uses the finite element method to solve the two-dimensional heat transfer forward problem. The finite element method does not directly calculate the global domain but accumulates each element to obtain the global quantity. Therefore, this article analyzes the unit volume. Since triangular elements have a strong ability to fit complex boundaries, triangular meshes are often used in finite element methods to divide the geometric domain of a two-dimensional system.

Fig. 1 illustrates a three-node triangular element. The three vertices in the triangular element are selected as the interpolation nodes of the temperature field.

The three-node element temperature field interpolation function is:

$$T = a_1 + a_2 x + a_3 y \tag{1}$$

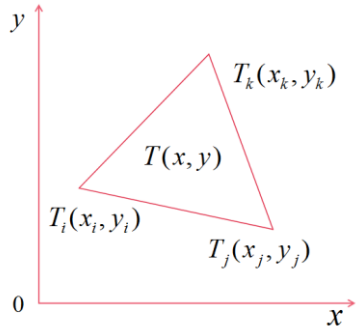

Fig. 1. Interpolation indication

where, T denotes the temperature at any point in the triangle mesh; a_1, a_2, a_3 are undetermined coefficients. To determine the three coefficient values in the equation, the temperature data of the three vertices of the triangle mesh is substituted into equation (1) to obtain the coefficient equation system:

$$\begin{aligned} T_i &= a_1 + a_2 x_i + a_3 y_i \\ T_j &= a_1 + a_2 x_j + a_3 y_j \\ T_k &= a_1 + a_2 x_k + a_3 y_k \end{aligned} \tag{2}$$

The solution is:

$$\begin{bmatrix} a_1 \\ a_2 \\ a_3 \end{bmatrix} = \frac{1}{2A} \begin{bmatrix} a_i & a_j & a_k \\ b_i & b_j & b_k \\ c_i & c_j & c_k \end{bmatrix} \begin{bmatrix} T_i \\ T_j \\ T_k \end{bmatrix} \tag{3}$$

where, A represents the area of the triangle mesh. Substituting equation (3) into equation (1), the temperature interpolation function of the triangular grid can be obtained:

$$T=\frac{1}{2A}\left[(a_i+b_ix+c_iy)T_i+(a_j+b_jx+c_jy)T_j+(a_k+b_kx+c_ky)T_k\right] \tag{4}$$

And equation (4) can be simplified as:

$$T=T_iN_i+T_jN_j+T_kN_k \tag{5}$$

where, N_i, N_j, and N_k are the vertex shape functions of the triangle mesh. The temperature field interpolation function of equation (5) can be used in the entire triangular grid domain, and the temperature field interpolation function on the element side can be simplified as shown in Fig. 2:

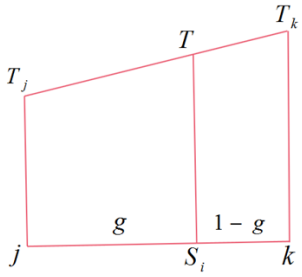

Fig. 2. Element side processing

As presented in Fig. 2, suppose *jk* is a boundary edge. The temperature of the point on the edge has nothing to do with T_i while it has a linear combination of the two points of *j*,*k*:

$$T=(1-g)T_j+gT_k \qquad 0\le g\le 1 \tag{6}$$

where, *g=0* corresponds to point *j*, and *g=1* corresponds to point *k*. When the triangle *jk* is the boundary side, the Galerkin weight function on the boundary can be obtained from equation (6):

$$\begin{aligned}\omega_i&=\frac{\partial T}{\partial T_i}=0\\ \omega_j&=\frac{\partial T}{\partial T_j}=1-g\\ \omega_k&=\frac{\partial T}{\partial T_k}=g\end{aligned} \tag{7}$$

After the domain is discretized by dividing it into each triangular mesh, the weighted integral margin on each element can be obtained:

$$R_l^e=\iint_e\left[\lambda\left(\frac{\partial\omega_l}{\partial x}\frac{\partial T}{\partial x}+\frac{\partial\omega_l}{\partial y}\frac{\partial T}{\partial y}\right)-\omega_lq+\omega_l\rho c\frac{\partial T}{\partial t}\right]d_xd_y-\oint_{\partial_e}\lambda\omega_l\frac{\partial T}{\partial n}ds \qquad l=1,2...n \tag{8}$$

where, *e* is the cell domain, ∂_e is the cell boundary, and ω_l is a known weighting function.

2.2. Boundary conditions solving

Introduce the first type of boundary conditions:

$$T=f(x,y,t) \tag{9}$$

The second type of boundary conditions:

$$q = -\lambda \frac{\partial T}{\partial n} \tag{10}$$

The third type of boundary conditions:

$$-\lambda \frac{\partial T}{\partial n} = h(T - T_f) \tag{11}$$

where, T denotes the temperature, $f(x, y, z, t)$ is a known mathematical function or constant, T_f is the surrounding environment, h is the surface heat transfer coefficient, λ is the thermal conductivity of the object, and n is the normal vector outside the boundary.

According to equation (9), when edge jk is in the first type of boundary condition, the boundary node temperature of the element should be a given value:

$$T_J = \overline{T}_j \qquad T_k = \overline{T}_k \tag{12}$$

$\overline{T}_j$, $\overline{T}_k$ is a known node temperature value, and the two-point values are usually equal. When the edge is in the second type of boundary condition, the node load of the element can be obtained by substituting equation (7) and equation (10) into equation (8):

$$\begin{aligned}
\Delta p_i &= \int_{jk} \omega_i \lambda \frac{\partial T}{\partial n} ds = -\int_{jk} q \omega_i ds = 0 \\
\Delta p_j &= \int_{jk} \omega_j \lambda \frac{\partial T}{\partial n} ds = -\int_0^1 (1-g) q s_i dg = -\frac{1}{2} q s_i \\
\Delta p_k &= \int_{jk} \omega_k \lambda \frac{\partial T}{\partial n} ds = -\int_0^1 g q s_i dg = -\frac{1}{2} q s_i
\end{aligned} \tag{13}$$

where, q is the boundary heat flux density. When edge jk is in the third type of boundary condition, it can be obtained by substituting equation (7) and equation (11) into equation (8):

$$\begin{aligned}
&\int_{jk} \omega_i \lambda \frac{\partial T}{\partial n} ds = \int_{jk} \omega_i h(T - T_f) ds = 0 \\
&\int_{jk} \omega_j \lambda \frac{\partial T}{\partial n} ds = \int_0^1 (1-g) h[(1-g)T_j + gT_k - T_f] s_i dg = h s_i (\frac{1}{3} T_j + \frac{1}{6} T_k - \frac{1}{2} T_f) \\
&\int_{jk} \omega_k \lambda \frac{\partial T}{\partial n} ds = \int_0^1 g h[(1-g)T_j + gT_k - T_f] s_i dg = h s_i (\frac{1}{6} T_j + \frac{1}{3} T_k - \frac{1}{2} T_f)
\end{aligned} \tag{14}$$

2.3. Time domain difference

In this paper, the forward heat transfer simulation of a pipe is a transient heat transfer, and the solution conditions include initial conditions, boundary conditions and a time difference. If the time is long enough it can be interpreted as steady state heat transfer, that is the temperature does not change with time, but the process evolves over time, so the time domain difference component is added.

The heat transfer region is discretized into N cells, that is :

$$\Omega \to \sum_{n} \Omega^{e} \tag{15}$$

The temperature field within the cells is interpolated using the temperature at the nodes, that is $T = N \cdot T_e$, then the variational generalization of the heat transfer problem is:

$$\Pi = \sum_{n} (\frac{1}{2} (T)^T (\lambda + h) T + [T]^T \left(c \frac{\partial T}{\partial t} - P \right)) \tag{16}$$

$$K = \int_{\Omega} \lambda (\nabla N)^T (\nabla N) d\Omega, \; h = \int_{s} h N^T N dA \tag{17}$$

$$C = \int_{\Omega} c \rho N^T N d\Omega, \; P = \int_{\Omega} q N^T d\Omega + \int_{S} q N^T dA + \int_{S} h T_f N^T dA \tag{18}$$

Fig. 3 exhibits the time domain difference of the finite element method:

Δt is the time step. The calculation of the backward difference format of the finite element is written as:

$$\frac{\partial T(t)}{\partial t} \approx \frac{T(t) - T(t - \Delta t)}{\Delta t} \tag{19}$$

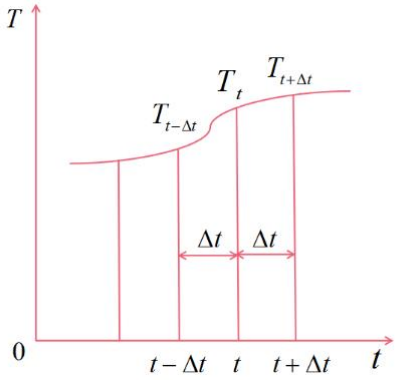

Fig. 3. Differential indication

Taking the extremes of the above generalized variation, that is $\partial \prod / \partial T = 0$, obtain the set of finite element equations : $C(\partial T / \partial t) + KT(t) = P(t)$. After adopting the backward difference format, the finite element heat transfer model can be written as:

$$\{T(t)\} = (K + \frac{C}{\Delta t})^{-1} [\{P(t)\} + \frac{C}{\Delta t} \{T(t - \Delta t)\}] \tag{20}$$

where, K denotes the temperature stiffness matrix, C is the hot fusion matrix, and P represents the node temperature load column vector. After adopting the backward difference format, each step of the calculation process only needs the temperature value of the previous step. In the first step of the calculation, only the initial temperature value can be used to calculate the temperature distribution at each time within the defined domain.

2.4. Forward problem verification

The two-dimensional circular pipe heat transfer model provided in Fig. 4 is used to verify the forward problem. Γ1 is the outer surface of the circular pipe, Γ2 is the inner surface of the pipe. The

outer radius of the circular pipe is 100m, the inner radius is 80m, and the thermal conductivity of the material is $\lambda = 25(W/m{\cdot}K)$, density is $2600(kg/m^3)$, specific heat capacity is $4200 J/(kg{\cdot}K)$. Initial temperature $T_0 = 293.15\,K$ (20 ℃) for both the inner and outer surfaces of the circular tube for Type I boundary conditions. The inner surface temperature of the circular tube is constant and the outer surface temperature varies with the length of the tube wall, the expression is $30/(-1*10^6)*h+50$, h takes values from $0-1000m$.

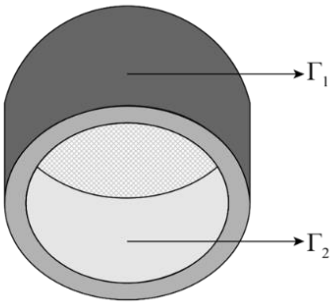

Fig. 4. Schematic diagram of circular pipe

The mathematical description of the two-dimensional tube heat transfer model is as follows:

$$\begin{cases} \dfrac{\partial^2 T}{\partial x^2} + \dfrac{\partial^2 T}{\partial y^2} = 0 \\ T = f_1(x,y,z,t) \quad \Gamma 1 \\ T = f_2(x,y,z,t) \quad \Gamma 2 \\ T = T_0 \quad \Omega \end{cases} \tag{21}$$

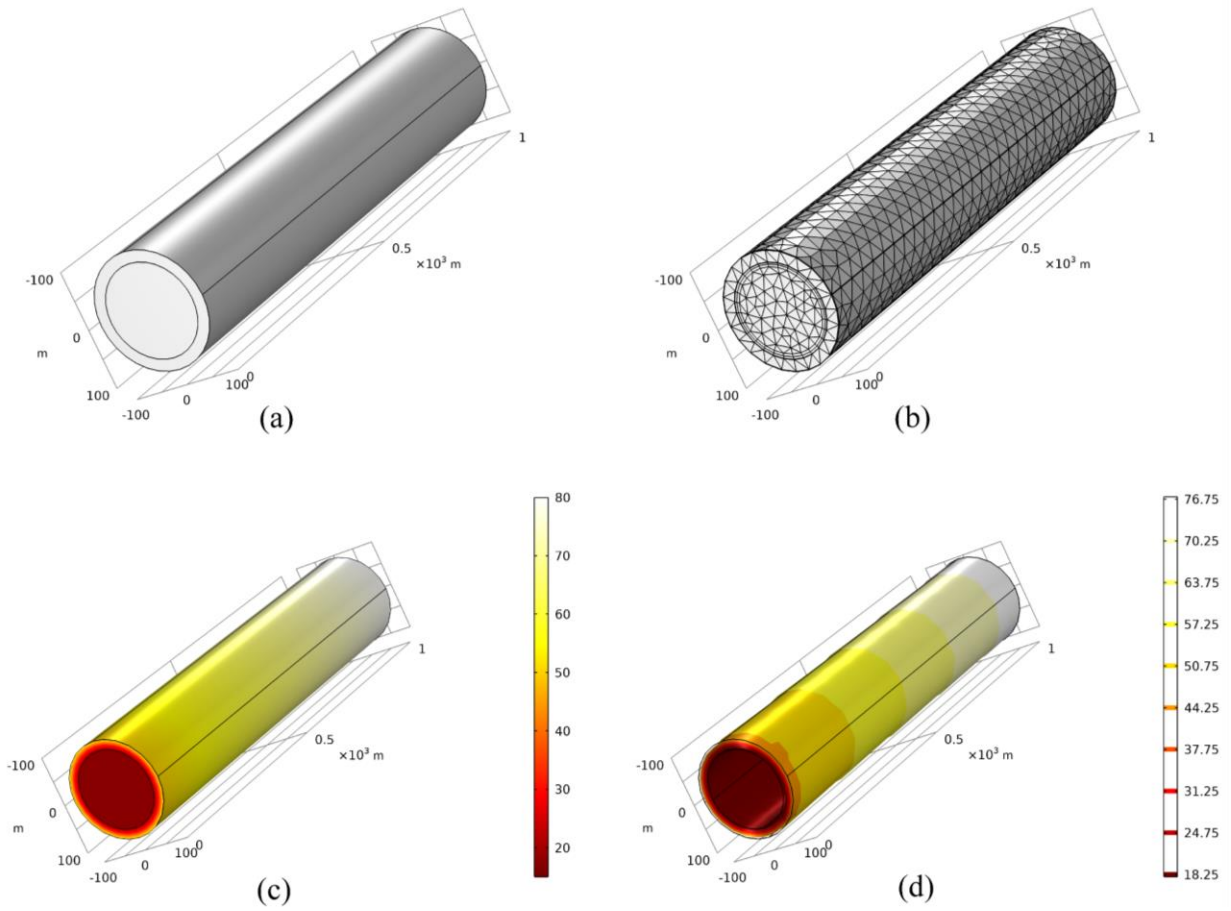

Fig. 5. Solving for the temperature field of a circular tube using finite elements

Fig. 5 shows the temperature field information solved for when the temperature information functions in the Γ1 and Γ2 planes are known. Fig. 5 (a) shows the 3D model created, with a circular tube 1000m long, Fig. 5 (b) shows the solved temperature using the finite element method, the meshing of the circular tube model, Fig. 5 (c) shows the solved temperature field information and Fig. 5 (d) shows the solved circular tube isotherm information.

From the solution of the circular tube, it is feasible to use the finite element method to realize the solution and analysis of the temperature field information distribution.

3. Two-dimensional inverse heat transfer problem

3.1. Inverse problem model

After verifying the feasibility of the finite element method using rectangular flat plates and circular tubes, the inverse problem follows the circular tube model described in the forward problem for inversion to identify defects on the inner wall of the pipeline. The idea of the inverse problem is to solve the geometry of the inner wall of the pipeline when the temperature information parameters of the outer wall of the pipeline are known. In the calculation of the inverse problem, a third type of boundary condition is added to both the inner and outer walls of the pipe, the surface heat transfer coefficient on the boundary of the circular tube and between the surrounding fluid is specified, as well as the temperature of the surrounding fluid, as shown in Fig. 6.

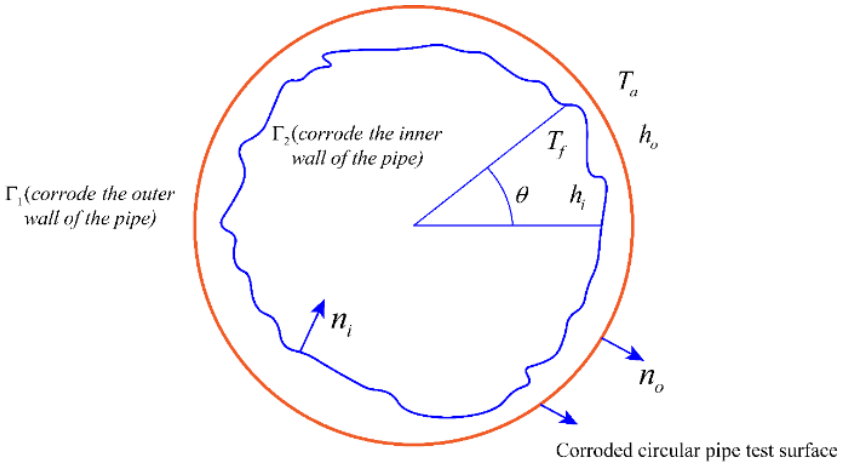

Fig. 6. Schematic diagram of the corroded pipeline

The mathematical model of the two-dimensional inverse heat transfer problem is described as follows:

$$\begin{cases} \dfrac{\partial^2 T}{\partial(\rho\cos\theta)^2}+\dfrac{\partial^2 T}{\partial(\rho\sin\theta)^2}=0 \\ -\lambda(\dfrac{\partial T}{\partial n_i})_2=h_i(T-T_f) \\ -\lambda(\dfrac{\partial T}{\partial n_o})_1=h_o(T-T_a) \end{cases} \tag{22}$$

where, λ is the thermal conductivity of the tube, n_i is the unit normal vector of the inner surface of the tube, n_o is the unit normal vector of the outer surface of the tube, h_i is the surface heat transfer coefficient of the inner surface of the tube, h_o is the surface heat transfer coefficient of the outer surface of the tube, T_f is the temperature of the fluid inside the tube, and T_a is the temperature of the fluid outside the tube. These thermophysical parameters are all known quantities.

It can be observed from the above-mentioned pipeline model and the schematic diagram that there is only one unknown quantity in equation (22), that is, the geometric shape of the inner surface 1 of the pipeline after corrosion, and the remaining parameters are known. Due to the complex geometry of the inner wall after corrosion, it is difficult to solve in the Cartesian coordinate system. To facilitate the following research, the following will adopt the polar coordinate system to describe the geometry of the inner wall, denoted by $P(\theta)$, and the temperature distribution on the outer surface of the tube is represented by the vector $Y=(Y_i, i=1,2,\ldots m)$. Therefore, the solution of the inverse problem can be understood as a process to make the error function accuracy close enough, that is, there is a sufficiently small search objective function $S(p)$, and its calculation formula is:

$$S_{(p)}=\sum_{i=1}^{m}(Y_i-T_i)^2 \tag{23}$$

where, p is the vector composed of the discrete radius r of the inner wall of the tube, that is, the estimated value of the function $P(\theta)$; m is the number of sampling points for the round tube; T_i is the temperature field calculated from p; Y_i is the true value of the temperature field.

3.2. Solving two-dimensional inverse heat transfer problem based on the conjugate gradient method

In the solution of the inverse heat transfer problem, the more classic conjugate gradient method is used[26-27]. The conjugate gradient method is a method between the steepest descent method and the Newton method. It improves the lack of slow convergence of the steepest descent method while avoiding the shortcomings of Newton's method of occupying large storage and complicated calculations.

In the process of iterative algorithm solving, there are several parameter conditions that need to be determined:

（1）Determine the conjugate search direction. It is a linear combination of the gradient direction of the objective function and the previous search direction, and its calculation formula is:

$$P^n(\theta) = \nabla S(p^n) + \gamma^n P^{n-1} \tag{24}$$

where, $\nabla S(p^n)$ is the descending gradient of the objective function, and γ^n is the conjugate coefficient when iterating to *n* steps. Its calculation formula is:

$$\gamma^n = \begin{cases} \dfrac{\sum_{i=1}^{m}\left[\nabla S(p^n)\right]_i^2}{\sum_{i=1}^{m}\left[\nabla S(p^{n-1})\right]_i^2} & n>0 \\ 0 & n=0 \end{cases} \tag{25}$$

$$\nabla S(p^n) = (\partial J/\partial p_1, \partial J/\partial p_2, \cdots \partial J/\partial p_m)$$

（2）Determine the search step factor. Its calculation formula is:

$$\beta^n = \frac{\sum_{i=1}^{m}\left[\left(T_i - Y_i\right)\left(P^n \frac{\partial T_i}{\partial p^n}\right]\right.}{\sum_{i=1}^{i=m}\left(P^n \frac{\partial T_i}{\partial p^n}\right)^2} \tag{26}$$

（3）Determine the termination condition of the iteration. Its calculation formula is:

$$S(P) = \sum_{i=1}^{m}(Y_i - T_i)^2 < \varepsilon \tag{27}$$

where, ε is the allowable error of discriminating convergence, generally a very small forward number. In actual engineering problems, errors are often difficult to avoid. Therefore, the termination condition with error can be written as:

$$S(P) = \sum_{i=1}^{m}(Y_i - T_i)^2 < m\sigma^2 \tag{28}$$

where, σ represents the standard deviation of the temperature measurement error. After determining the above parameters, the formula for identifying the internal defects of the corroded tube can be written as:

$$P^{n+1} = P^n - \beta^n P^n \tag{29}$$

Therefore, the geometric shape of the inner wall of the corroded tube can be solved iteratively through equation (26).

3.3. The introduction of the firefly algorithm

Considering the large fluctuations in the data of some sampling points, the Firefly Algorithm[28] (FA) is introduced to randomly optimize the data[29-31].

Mathematical description of FA:

（1）Relative fluorescence brightness of fireflies

$$I = I_0 e^{-\omega r_{ij}} \tag{30}$$

where, I_0 is the brightness of the brightest firefly, that is, the brightness of itself (where r=0); ω refers to the light absorption coefficient, which can be set as a constant; r_{ij} represents the distance between firefly *i* and *j*.

（2）Mutual attraction

$$v(r) = v_0 e^{-\gamma r_{ij}^2} \tag{31}$$

where, V_0 represents the maximum attraction, that is, the attraction at the light source (r=0).

（3）Optimal target iteration

$$adi(t+1) = adi(t) + v(adj(t) - adi(t)) + \alpha(rand - 1/2) \tag{32}$$

where, adi and adj represent the spatial positions of the two fireflies *i* and *j* , respectively; α is the spatial step size; rand is a random factor that obeys a uniform distribution on [0,1].

When performing stochastic optimisation of temperature information, some basic parameters of the firefly optimisation algorithm were set as follows: the population size was set to 100, the initial fluorescein concentration was set to 5, the volatility factor of fluorescein was set to 0.4, the enhancement factor of fluorescein was set to 0.5, the domain change rate was set to 0.06, and the adaptation extraction ratio was set to 0.06.

Flow chart of the hybrid algorithm after the introduction of FA in presented in Fig.7.

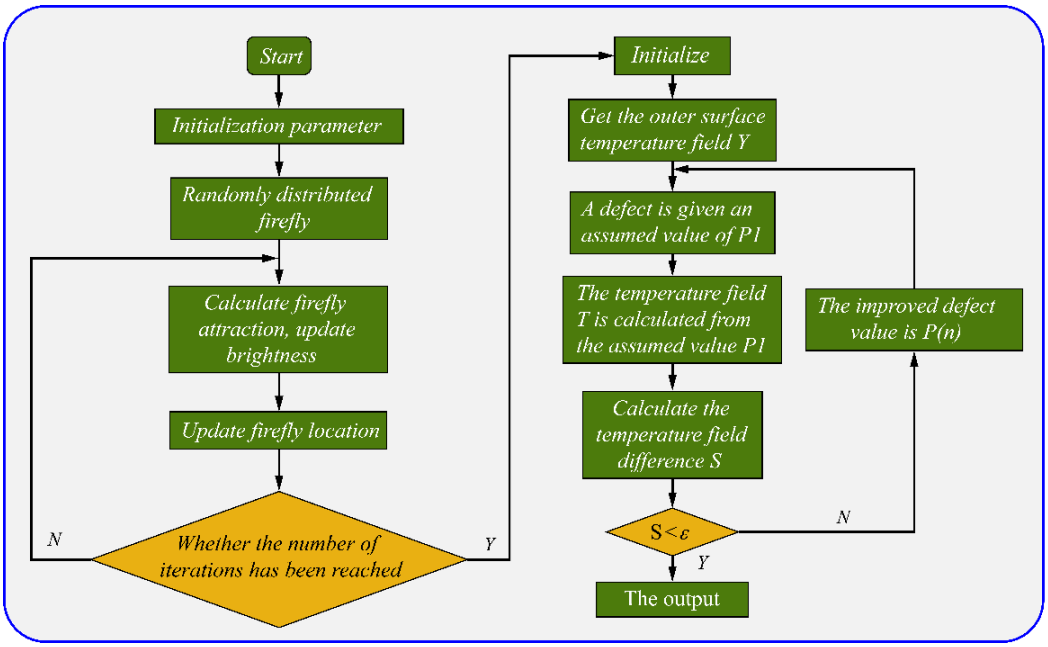

Fig. 7. Algorithm flow chart

3.4. Numerical experiment and analysis

In this paper, the aforementioned circular tube model is used for numerical experiments, two kinds of corrosion of the inner wall surface are considered, and the influence of the different number of measurement points and measurement errors on the experiment is analyzed[32]. The radius of the outer wall of the pipe is 0.18m, the radius of the inner wall is 0.13m, the thermal conductivity of the material is $\lambda = 25(W/m*K)$, and the convective heat transfer coefficient of the inner wall is $h_i = 1000(W/m^2*K)$. The outer wall is natural convection. Assuming that the inner wall parameters after two kinds of corrosion are as follows:

The first type of inner wall corrosion defect:

$$r_1 = \begin{cases} 0.130 & (0 \le \theta < \frac{2\pi}{3} \bigcup \frac{4\pi}{3} < \theta \le 2\pi) \\ 0.165 & (\frac{2\pi}{3} \le \theta \le \frac{4\pi}{3}) \end{cases} \tag{33}$$

The second type of inner wall corrosion defect:

$$r_2 = 0.03*\sin(\theta) + 0.130 \qquad (0 \le \theta \le 2\pi) \tag{34}$$

Take the first type of corrosion of the inner wall boundary as an example, at the number of measurement points N=20, consider the effect of different measurement errors on the experimental results, respectively take $\sigma = 0.01, 0.2, 0.4$ for the simulation experiments.

The identification results using the conjugate gradient method are shown in Fig. 8.

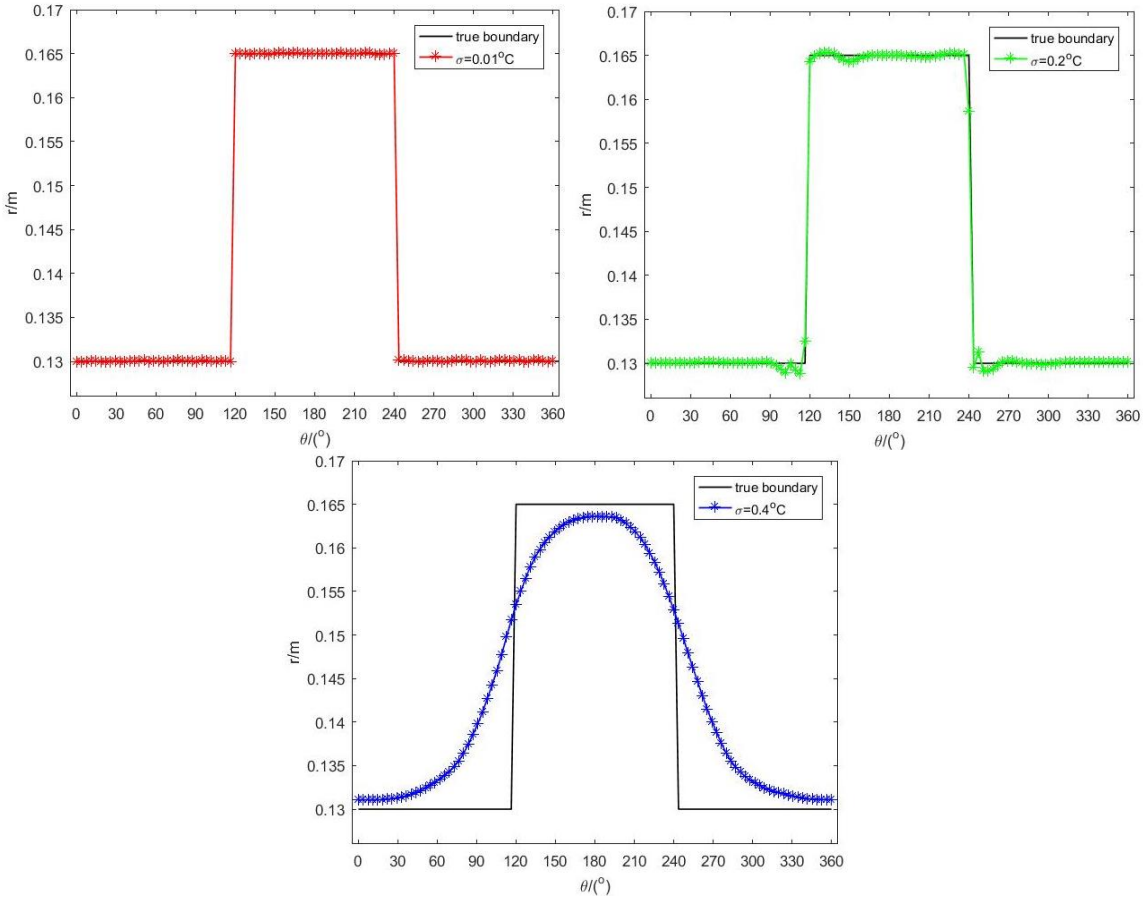

Fig. 8. The inversion result of the first boundary single algorithm

Table 1. The error value of the inversion result of a single algorithm under different measurement errors

Measurement error σ	0.01	0.2	0.4
Relative mean error $\eta\%$	0.08	0.76	7.58

It can be observed from Table 1 and Fig. 8 that the inversion accuracy is highest when the measurement error is $\sigma = 0.01$. As the measurement error increases, the fluctuation of the inversion value increases. When $\sigma = 0.4$, the geometric shape of the inner wall can only be roughly recognized.

The recognition result after introducing FA for random optimization is illustrated in Fig. 9:

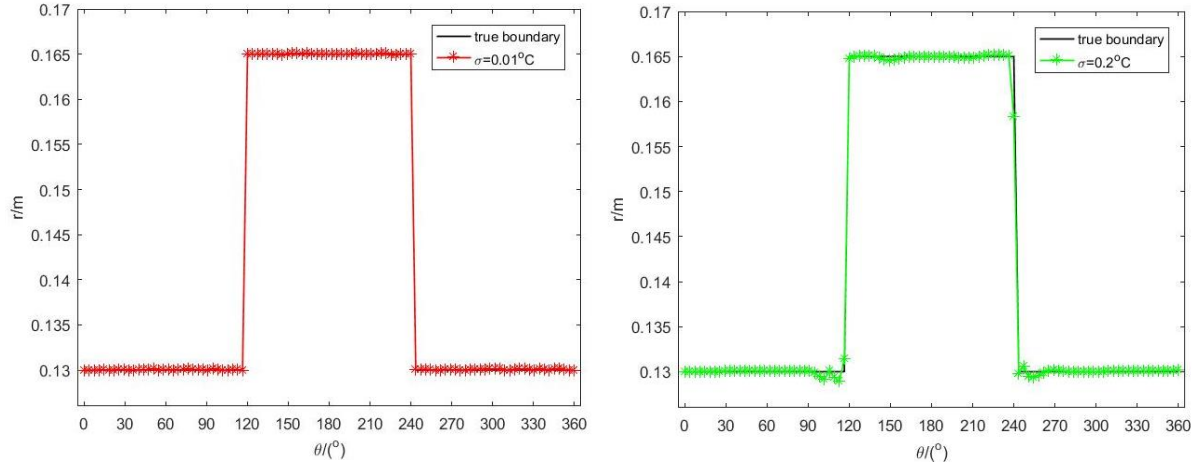

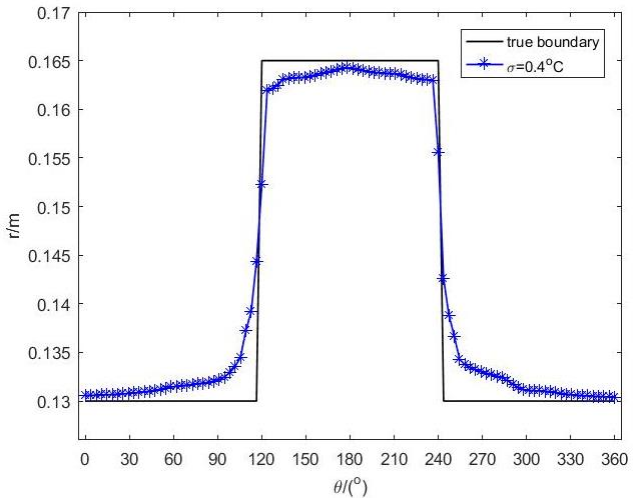

Fig. 9. The first boundary inversion result after the introduction of FA

Table 2. Error values of inversion results after introducing FA under different measurement errors

Measurement error σ	0.01	0.2	0.4
Relative mean error $\eta\%$	0.05	0.49	3.41

It can be revealed from the comparison of Tables 1 and 2 and Fig. 8 and 9 that after the introduction of FA, the fluctuation of some data values is suppressed to a certain extent. Particularly, the image changes when $\sigma = 0.4$ is the most significant, and the inversion accuracy is greatly improved. However, the inversion value still fluctuates greatly when the shape of the inner wall defect occurs abruptly; thus, it needs to be further improved.

In the following content, the second type of corrosion of the inner wall boundary is used as an example (introducing FA), and the influence of the number of measured nodes *N* on the experimental results is considered. Perform simulation experiments when *N=14,28,56* , respectively:

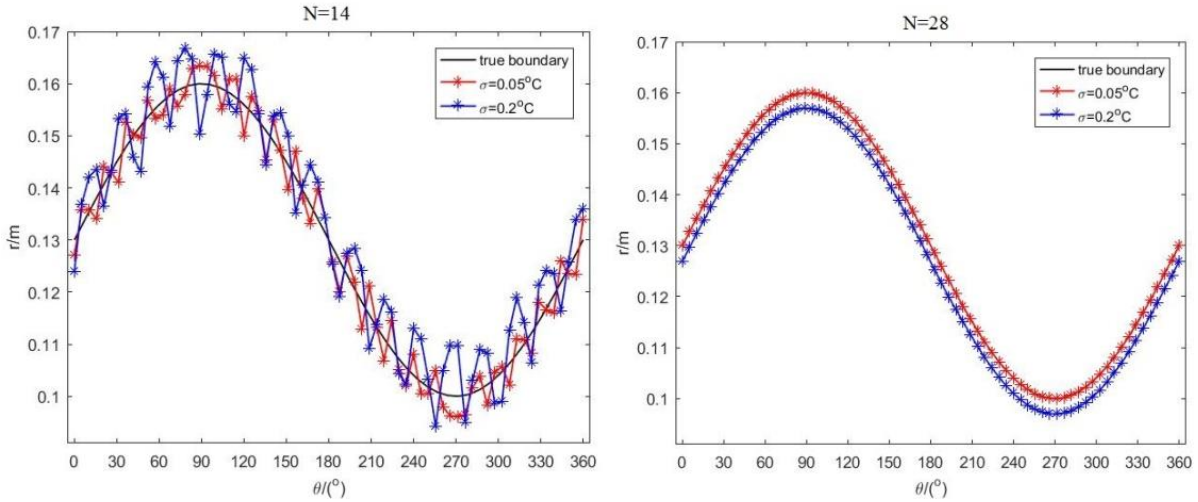

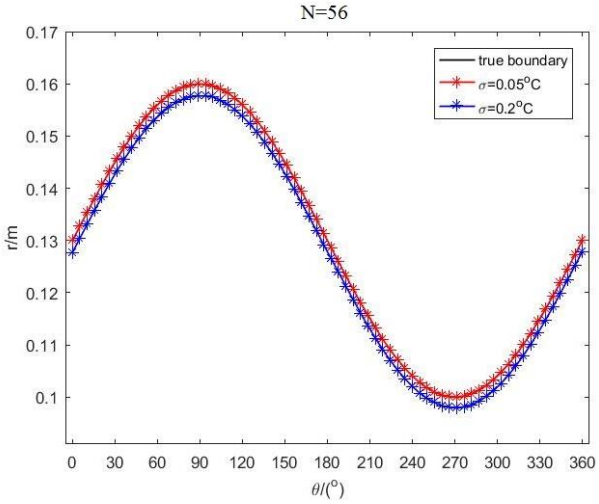

Fig. 10. The second boundary inversion result

Table 3. Error values of inversion results under different number of measuring points

Number of measuring point N	14		28		56	
Measurement error σ	0.05	0.2	0.2	0.05	0.2	0.05
Relative mean error $\eta\%$	2.84	6.13	0.04	2.57	0.03	1.95

As indicated from Table 3 and Fig. 10, the measurement information is deficient when the number of measurement points N is 14; The inversion result has certain fluctuations when $\sigma = 0.05$; The inversion result fluctuates more and the deterioration magnifies significantly when $\sigma = 0.2$. Moreover, a more accurate inversion result is obtained when the number of measuring points N is 28. The inversion accuracy is further improved when the number of measuring points N changes from 28 to 56.

4. Conclusions

In this paper, the geometric shape of the inner wall of the two-dimensional steady-state circular pipe is inverted by the finite element method and the conjugate gradient method optimized by firefly：

1. For the forward heat conduction problem in this paper, after the feasibility of the algorithm is proved by taking circular pipe as objects, the finite element method is used to solve the analysis. Simulation results show that the algorithm has good stability and improves the efficiency of numerical experiments.

2.The analysis and solution of numerical experiments verify that the method in this paper has high accuracy in the inversion process. Meanwhile, the influence of the different number of measuring points and measuring error on the experimental results is discussed. It is demonstrated that two different types of corrosion on the inner wall of the tube can be effectively identified when there is a certain measurement error or basic temperature information of the measuring point.

3.The conjugate gradient algorithm is used to identify the geometric shapes of the corroded inner walls of two pipelines. After finding that the recognition effect is not particularly ideal at the mutation of the objective function, the firefly algorithm is introduced to optimize the processing of temperature information based on the conjugate gradient algorithm. This further improves the stability of the inversion results compared to the conjugate gradient method.

Nomenclature

T	temperature (K)	a	undetermined coefficient (-)
A	area of mesh (m^2)	jk	boundary edge (m)
N	functions of the mesh (-)	T_f	ambient temperature (K)
T_a	temperature of the fluid (K)	h	heat transfer coefficient ($W/(m^2 \cdot K)$)
n	normal vector (-)	q	heat flux density ($J/(m^2 \cdot s)$)
K	temperature stiffness matrix (-)	C	hot fusion matrix (-)
P	node temperature load column vector (-)	$\nabla S(p^n)$	descending gradient (-)
Δt	time step (-)	ρ	density (kg/m^3)

Greek symbols

Γ	surface of the pipe (-)	σ	measurement error (-)
η	relative mean error (-)	λ	thermal conductivity ($W/(m \cdot K)$)
∂	cell boundary (-)	γ^n	conjugate coefficient (-)
ω_l	weighting function (-)		

Abbreviations

FEM	finite element method	CGM	conjugate gradient method
FA	firefly algorithm	DFIM	decentralized fuzzy inference method

Subscripts

e	cell domain	i,j,k	Mesh vertex position

References

[1] Wang, SB., *et al*., Solving of Two-Dimensional Unsteady-State Heat-Transfer Inverse Problem Using Finite Difference Method and Model Prediction Control Method, *Complexity, 2019* (2019), 7, pp. 1-12

[2] Gonzalez M., *et al*., Inverse geometry heat transfer problem based on a radial basis functions geometry representation, *International Journal for Numerical Methods in Engineering, 65* (2006), 8, pp. 1243-1268

[3] Lu, T., *et al*., A two-dimensional inverse heat conduction problem in estimating the fluid temperature in a pipeline, *Applied Thermal Engineering, 30* (2010), 13, pp. 1574-1579

[4] Szenasi, S., *et al*., Configuring Genetic Algorithm to Solve the Inverse Heat Conduction Problem, *Acta Polytechnica Hungarica, 14* (2017), 6, pp. 133-152

[5] Zhang, T., *et al*., Seeking heat source in inverse heat conduction problem by using particle swarm optimization, *University of Shanghai for Science and Technology, 04* (2013), pp. 377-381

[6] Peker, HA., *et al*., Application of Kashuri Fundo Transform and Homotopy Perturbation Methods to Fractional Heat Transfer and Porous Media Equations, *Thermal Science, 26*(2022), 4A, pp. 2877-2884

[7] Cuha,FA., *et al*., Solution of Abel's Integral Equation by Kashuri Fundo Transform, *Thermal Science, 26*(2022), 4A, pp. 3003-3010

[8] Peker,HA., *et al*., Solving steady Heat Transfer Problems via Kashuri Fundo Transform, *Thermal Science, 26*(2022), 4A, pp. 3011-3017

[9] Jiang, S., *et al*., Geometry Estimation of Furnace Inner Wall Based on BEM and Decentralized Fuzzy InferenceMethod, *World Sci-Tech R&D, 65* (2006), 8, pp. 122-126
[10] Luo, Z., *et al*., Fuzzy Estimation for Irregular Configuration of Furnace, *Journal of engineering thermophysics, 10* (2013), 8, pp. 1906-1909
[11] Wang, D., Thermal Conducting Geometric Inversion Method Based on the Third Boundary Condition, Ph. D. thesis, Harbin Institute of Technology, Harbin, China, 2018
[12] Li, Y., Non-Iterative Algorithm for Identifying Boundary Conditions and Geometry Shapes in Heat Conduction Problems, Hefei University of Technology, Hefei, China, 2018
[13] Wang, S., *et al*., Two-Dimensional Steady-State Boundary Shape Inversion of CGM-SPSO Algorithm on Temperature Information, *Science Citation Index, 2017* (2017), pp. 1-12
[14] Mei, L., *et al*., A New Method to Evaluate the Subsurface Defect by Thermal Nondestructive Testing, *Infrared Millim Waves, 06* (2000), pp. 457-459
[15] Sun, S., *et al*., Back Calculation for Cold-state Geometric Shape of Turbine Blade Based on Modification of Nodal Coordinates and Mesh Smoothing, *Journal Of Mechanical Engineering, 50* (2014), 10, pp. 143-148
[16] Fazeli, H., *et al*., Mirzaei M. Shape identification problems on detecting of defects in a solid body using inverse heat conduction approach, *Journal of mechanical science and technology, 26* (2012), pp. 3681-3690
[17] Fazeli H., *et al*., Estimation of Location and Size of Defects in a Solid Body via Inverse Heat Conduction Problem, *International Heat Transfer Conference*, 2006, pp. 387-396
[18] Li, Y., *et al*., A decentralized fuzzy inference method for the inverse geometry heat conduction problem, *Applied Thermal Engineering, 106* (2016), 8, pp. 109-116
[19] Cheng, CH., Cheng, MH., Shape Identification by Inverse Heat Transfer Method, *Journal of Heat Transfer, 125* (2013), 2, pp. 224-231
[20] Mosavati, M., *et al*., A Novel, Noniterative Inverse Boundary Design Regularized Solution Technique Using the Backward Monte Carlo Method, *Journal of Heat Transfer, 135* (2013), 4, pp. 130-136
[21] Mosavati, B., *et al*., Solution of radiative inverse boundary design problem in a combined radiating-free convecting furnace, *International Communications in Heat and Mass Transfer, 45* (2013), pp. 130-136
[22] Mosavati, B., *et al*., Inverse boundary design solution in a combined radiating-free convecting furnace filled with participating medium containing specularly reflecting walls, *International Communications in Heat and Mass Transfer, 76* (2016), pp. 69-76
[23] Chen, W., Yang, Y., Inverse estimation for unknown fouling-layer profiles with arbitrary geometries on the inner wall of a forced-convection duct, *International Journal of Thermal sciences, 49* (2010), 1, pp. 86-98
[24] Fan, C., *et al*., Research on the recognition algorithm of irregular boundary of inner wall of circular tube based on infrared temperature measurement, *Journal of Thermal Science and Technology, 02* (2006), pp. 112-117
[25] Partridge PW., Wrobel L C ., An inverse geometry problem for the localisation of skin tumours by thermal analysis, *Engineering Analysis with Boundary Elements, 31* (2007), 10, pp. 803-811
[26] Zhu, L., *et al*., Estimating Steady Multi-variables Inverse Heat Conduction Problem by Using Conjugate Gradient Method, *Proceedings of the CSEE, 31* (2011), 8, pp. 58-61

[27] Zhang, YW., *et al*., Inverse Heat Conduction Problem of Deducing Inner Wall Temperature by Using Conjugate Gradient Method, *Journal Of Engineering Thermophysics, 30* (2009), 7, pp. 1188-1190
[28] Yang, XS., Firefly algorithm, stochastic test functions and design optimization, *International Journal of Bio-Inspired Computation, 2*(2010), 2, pp. 78-84
[29] Ma, X., *et al*., Energy-Saving Operation Optimization of High-Speed Trains Using Firefly Algorithm, *Journal of Huaqiao University(Natural Science), 4* (2019), pp. 452-456
[30] Zuo, Z., *et al*., An Improved Swarm Optimization Alogorithm, *Microelectronics & Computer, 35* (2018), 2, pp. 61-66
[31] Gao, W., Study on the Firefly Algorithm and Application, Lanzhou University, Lanzhou, China, 2013
[32] Lu, S., *et al*., Identification of irregular pipeline geometry boundary using infrared transient inspection based on finite element discretization, *CIESC Journal, 63* (2012), 12, pp. 3805-3811

Paper submitted: 30.12.2022
Paper revised: 30.01.2023
Paper accepted: 08.02.2023